# Ultrahigh Density Alignment of Carbon Nanotube Arrays by Dielectrophoresis

**Shashank Shekhar,[†,‡] Paul Stokes,[†,‡] and Saiful I. Khondaker[†,‡,§,*]**

[†]Nanoscience Technology Center, [‡]Department of Physics, and [§]School of Electrical Engineering and Computer Science, University of Central Florida, Orlando, Florida 32826, United States

**ABSTRACT** We report ultrahigh density assembly of aligned single-walled carbon nanotube (SWNT) two-dimensional arrays *via* AC dielectrophoresis using high-quality surfactant-free and stable SWNT solutions. After optimization of frequency and trapping time, we can reproducibly control the linear density of the SWNT between prefabricated electrodes from 0.5 SWNT/$\mu$m to more than 30 SWNT/$\mu$m by tuning the concentration of the nanotubes in the solution. Our maximum density of 30 SWNT/$\mu$m is the highest for aligned arrays *via* any solution processing technique reported so far. Further increase of SWNT concentration results in a dense array with multiple layers. We discuss how the orientation and density of the nanotubes vary with concentrations and channel lengths. Electrical measurement data show that the densely packed aligned arrays have low sheet resistances. Selective removal of metallic SWNTs *via* controlled electrical breakdown produced field-effect transistors with high current on−off ratio. Ultrahigh density alignment reported here will have important implications in fabricating high-quality devices for digital and analog electronics.

**KEYWORDS:** carbon nanotube · directed assembly · solution processed · array

Single-walled carbon nanotubes (SWNTs) are considered to be a promising building block for future digital and analog electronic circuits due to their exceptional electronic properties.[1,2] Electron transport measurements of devices fabricated from individual SWNTs have displayed subthreshold swings as low as 60 mV/decade, mobilities reaching 79 000 $cm^2/(V \cdot s)$, and conductance nearing the ballistic limit ($G = 4e^2/h \sim 155\ \mu S$ or $R \sim 6.5$ k$\Omega$).[3,4] One of the main challenges in nanotube electronics is the chirality control of the individual SWNT which causes large device-to-device inhomogeneity in performance. Devices fabricated from arrays of SWNTs can be advantageous over individual tube devices, as they may provide more homogeneity from device to device and can cover large areas. In addition, devices fabricated with nanotube arrays contain hundreds of parallel SWNTs contributing to charge transport, which can increase current outputs up to hundreds of microamperes. Aligned arrays of SWNTs are also of particular interest in radio frequency (RF) applications as they may provide the higher cutoff frequency in the terahertz regime and low input impedance (~50 $\Omega$).[5] In addition, the degree of alignment and the density of SWNTs have a great influence on device performance. Compared to multilayered arrays and random films, where tube−tube junction limits charge transport, a perfectly aligned two-dimensional (2D) array of SWNTs is expected to exhibit electronic properties that approach the intrinsic properties of an individual nanotube. Due to these advantages, there is a push to fabricate devices with massively parallel 2D arrays of SWNTs.[5−25] Such devices may be useful for radio frequency applications,[5−7,15,26] transistors,[10] plastic electronics,[10−12] display technologies,[27−29] and sensors.[30]

Several techniques are being developed for the fabrication of dense aligned arrays of SWNTs. Direct growth *via* chemical vapor deposition (CVD) using pattern lines of catalyst on single crystal quartz or sapphire substrate achieved an aligned array with an average linear density of ~10 SWNT/$\mu$m using single growth technique[10,17] and ~30 SWNT/$\mu$m using more complicated double growth technique.[18] However, direct growth technique requires very high temperature (~900 °C), and transfer printing is required to transfer the aligned array to suitable substrates for device fabrication.[6,10,14] Post-growth assembly using a solution processed SWNT could be advantageous due to its ease of processing at room temperature, compatibility with current complementary metal oxide semiconductor fabrication, and potential for scaled up manufacturing of SWNT devices on various substrates. Among the post-growth techniques, Langmuir−Blodgett assembly,[19] bubble blown assembly,[20] evaporation-driven self-assembly,[22] spin coating assisted alignment,[23] and contact printing[24] have demonstrated reasonably high density alignment with ~1 SWNT/$\mu$m in most cases and up to 10 SWNT/$\mu$m in a few cases.

One technique that has the potential to assemble SWNTs with ultrahigh density

* Address correspondence to saiful@mail.ucf.edu.

Received for review September 6, 2010 and accepted February 8, 2011.

**Published online February 16, 2011**
**10.1021/nn102305z**

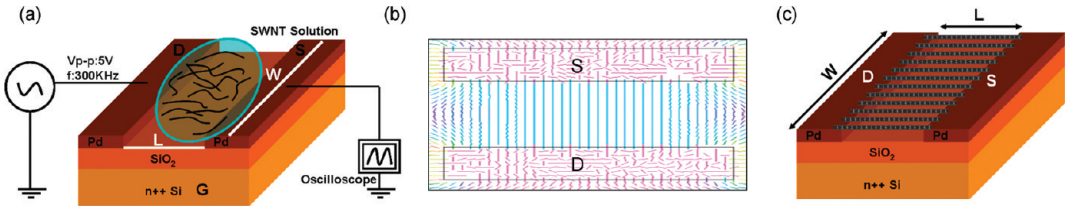


**Figure 1. (a) Schematic of the DEP assembly. (b) Two-dimensional simulated electric field around the electrode gap. S and D are Pd source and drain electrodes. (c) Cartoon of the aligned nanotubes after the DEP process. By varying the concentration of SWNT solution, the number density of the assembled nanotubes can be tuned.**

alignment is AC dielectrophoresis (DEP).[8,25,31,32] DEP has been used to assemble 2D, 1D, and 0D nanomaterials at the selected position of the circuit for device applications.[32−38] DEP can be advantageous over other solution processed techniques because it allows the materials to be directly integrated to prefabricated electrodes at the selected positions of the circuits and does not require post-etching or transfer printing. One crucial aspect of the DEP process for high density alignment is the quality of the SWNT solution. The solution should be free of catalytic particles, contain mostly individual SWNTs, and be stable for long periods of time. Catalytic particles in the solution tend to make their way into the electrode gap with the SWNTs during the assembly process due to their highly conductive nature which can disrupt the assembly and degrade device performance. Solutions containing bundles make it difficult to obtain only individual SWNTs reproducibly into the electrode gap as the DEP force will likely select the larger bundles due to their higher dielectric constant and conductivity.

In this paper, we used a clean, surfactant-free, and stable SWNT aqueous solution combined with the DEP technique to achieve ultrahigh density alignment of SWNTs in an array. The assembly was done by applying an AC voltage of 5 Vp-p at 300 kHz between prefabricated palladium (Pd) source and drain electrodes of channel lengths ($L$) of 2, 5, and 10 $\mu$m while channel width ($W$) was varied from 25 $\mu$m to 1 mm to show the scalability of the process. By simply tuning the concentration of the nanotubes in the solution, we can reproducibly control the linear density of the SWNT uniformly in the two-dimensional array from 0.5 SWNT/$\mu$m to more than 30 SWNT/$\mu$m. Our maximum density of 30 SWNT/$\mu$m is the highest reported density of aligned arrays *via* any solution processing technique. Further increase of SWNT concentration results in dense arrays with multiple layers. We discuss how the orientation and density of the nanotube vary with concentrations and channel lengths. Electrical measurement data show that the densely packed aligned arrays have sheet resistances of 3−10 kΩ/□. Selective removal of metallic SWNTs *via* controlled electrical breakdown produced field-effect transistors (FETs) with high current on−off ratio. Ultrahigh density alignment using solution processed SWNTs reported here will have important implications in fabricating high-quality nanoelectronic devices.

## RESULTS AND DISCUSSION

Figure 1a shows a cartoon of the DEP assembly setup. The channel lengths ($L$) were 2, 5, and 10 $\mu$m, while the channel width ($W$) was varied from 25 $\mu$m to 1 mm. The directed assembly of SWNTs at predefined electrodes was done in a probe station under ambient conditions *via* DEP. The SWNT aqueous solution was obtained from Brewer Science Inc., which was stable for at least 6 months.[39,40] The solution was free from surfactant, catalytic particles, and bundles and contained mostly individual SWNTs of average diameter ∼1.7 nm, while the length of the nanotubes varied from 0.3 to 10 $\mu$m with a mean value of 1.5 $\mu$m as determined from atomic force microscopy (AFM) and scanning electron microscopy (SEM) investigations (see Supporting Information). We have previously verified through DEP assembly of individual SWNTs and using room temperature and low temperature electronic transport measurements that the SWNTs obtained from the same source are of high quality.[36,37] The solution has an original SWNT concentration of ∼50 $\mu$g/mL and was diluted using deionized (DI) water to a desired concentration. Prior to the assembly, the substrates with patterned electrodes were placed in oxygen plasma cleaner for 10 min to remove any unwanted organic residues on the surface. For the assembly, a small (3 $\mu$L) drop of the SWNT solution was cast onto the chip containing the electrode arrays. An AC voltage of 5 Vp-p with a frequency of 300 kHz was applied using a function generator between the source and drain electrodes for 30 s. The AC voltage gives rise to a time averaged dielectrophoretic force. For an elongated object, it is given by $F_{DEP} \propto \varepsilon_m \mathrm{Re}[K_f] \nabla E^2_{RMS}$, $K_f = (\varepsilon^*_p - \varepsilon^*_m)/\varepsilon^*_m$, $\varepsilon^*_{p,m} = \varepsilon_{p,m} - i(\sigma_{p,m}/\omega)$, where $\varepsilon_p$ and $\varepsilon_m$ are the permittivity of the nanotube and solvent, respectively, $K_f$ is the Claussius−Mossotti factor, $\sigma$ is the conductivity, and $\omega = 2\pi f$ is the frequency of the applied AC voltage.[41] The induced dipole moment of the nanotube interacting with the strong electric field causes the nanotubes to move in a translational motion along the electric field gradient and align in the direction of the electric field lines. The DEP assembly depends mainly on four parameters: the applied external voltage (Vp-p), sinusoidal frequency ($f$), concentration of SWNT solution, and DEP time. In principle, the controlled alignment can be achieved by optimizing any of the above parameters. We found that the optimum nanotube assembly occurs between 300 kHz and 1 MHz and for 5−10 V. We observed

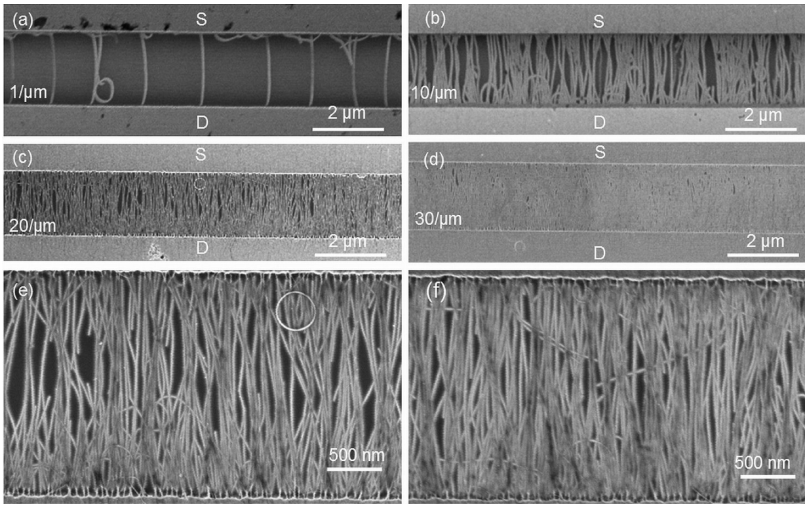


**Figure 2. Scanning electron microscopy (SEM) image for a typical DEP assembly with varying nanotube density: (a) ~1 SWNT/$\mu$m; (b) 10 SWNT/$\mu$m; (c) 20 SWNT/$\mu$m; and (d) 30 SWNT/$\mu$m. (e,f) Magnified image of (c) and (d). The nanotube density is varied by simply tuning the concentration of the solution while keeping all other DEP parameters fixed. For this assembly, $L$ = 2 $\mu$m and $W$ = 25 $\mu$m.**

that waiting for a period of 30 s resulted in homogeneous assembly and a better reproducibility.

Figure 1b shows a simulation of the electric field around the electrode gap for the parallel electrode patterns. The simulations were done using a commercially available software (Flex PDE) assuming that the potential phasor is real and therefore using the electrostatic form of the Laplace equation ($\nabla^2\Phi = 0$). Hence we can set the effective potential of the electrodes to $\Phi = \pm V_{p\text{-}p}/2$ for our simulation. As can be seen from the simulation, the electric field is uniform throughout the electrode gap, allowing for many nanotubes to align parallel to one another throughout the gap. After the assembly, the function generator was turned off and the sample was blown dry by a stream of nitrogen gas. Figure 1c shows the schematic of an array of assembled nanotubes.

Figure 2 shows SEM images for a typical DEP assembly when the concentration of the SWNT solution was varied by simply diluting the original solution using DI water. The electrode pairs have $L$ = 2 $\mu$m and $W$ = 25 $\mu$m. When the SWNT concentration was 0.08 $\mu$g/mL (diluted 600 times), on an average, there was 1 SWNT/$\mu$m assembled between the electrodes, as shown in Figure 2a. Figure 2b shows an image where the concentration was 0.34 $\mu$g/mL (diluted 150 times). From this image, we count an average of 10 SWNT/$\mu$m entirely bridging the two electrodes. As the concentration of the solution is increased to 1.67 $\mu$g/mL (30 times dilution) and 3.4 $\mu$g/mL (15 times dilution), we found that the linear density of the SWNT is increased to ~20 and ~30/$\mu$m, as shown in Figure 2c,d, respectively. A magnified view of these images is shown in Figure 2e,f. At low densities, almost all of the nanotubes are well-aligned and are parallel to each other. However, at higher density, about 90% are aligned within $\pm 10^\circ$ of the longitudinal axis (Figure 2e,f). As can be seen from these images, by simply varying the concentration of the SWNT solution, we are able to vary the density of the SWNT in the channel from 1 to ~30 SWNT/$\mu$m. The maximum density reported here is the highest for any solution processed technique and is comparable to double growth CVD technique, which was done at very high temperature (900 °C).[18] One crucial aspect of our alignment is that the density of the nanotube is uniform throughout the channel width. This uniformity of the SWNT can be attributed to the uniform electric field lines in a parallel plate arrangement. In addition, in contrast to previous DEP assemblies, our aligned nanotube array does not contain any bundle nor does it contain any catalytic particle. This is due to the high-quality SWNT solutions used in this study.

We have also investigated the effect of further increase of SWNT concentration in the solution for this channel length. When the concentration of SWNT was increased to 6.8 $\mu$g/mL (8 times dilution), the linear density of the SWNT increased to more than 30/$\mu$m, as shown in Figure 3a,b; however, we found that significant numbers of nanotubes form a second or even third layer, making the nanotube film 2−3 layers thick at certain places, as verified from AFM study. At 30 SWNT/$\mu$m, the inner nanotube separation is about 33 nm, and it is not clear why the inner nanotube separation cannot be further decreased without making multilayers. Further theoretical and experimental studies are required to elucidate this.

In order to demonstrate the scalability of the DEP assembly process, we have carried out similar alignment in larger channel length devices with $L$ = 5 and 10 $\mu$m by varying the concentration of the SWNT solution. This is shown in Figure 4, where the left panel is for $L$ = 5 $\mu$m and the right panel is for $L$ = 10 $\mu$m. The value of $W$ was kept fixed at 25 $\mu$m. Figure 4a shows the SEM image for the assembly when the concentration was 0.167 $\mu$g/mL (300 times dilution), which resulted in assembly of 20 SWNTs on the entire 25 $\mu$m channel width, giving a linear

density of 0.8 SWNT/$\mu$m. Figure 4b,c shows the alignment with a density of 8 and 28 SWNT/$\mu$m, respectively. These alignments were achieved by the solution concentrations of 0.83 $\mu$g/mL (60 times dilution) and 8.3 $\mu$g/mL (6 times dilution). The intermediate density alignments were also achieved by DEP using intermediate solution concentrations (images are not shown here). A small number of short nanotubes can also be seen at the bases of electrodes. This is mostly likely due to the alteration of the electric field near the electrode nanotube junctions from the already assembled nanotubes bridging the gap which modify the electric field lines and allow smaller nanotubes to gather around them (see Supporting Information for more detailed description).[38] In order to avoid such short nanotubes at the base, it will be necessary to find techniques where the smaller nanotubes can be filtered out from the solution. To further investigate the nature of alignment in large electrode separation, assembly was carried out on the device of $L$ = 10 $\mu$m. Figure 4d shows the SEM image of alignment with a density of 0.5 SWNT/$\mu$m. The concentration used for this assembly was 0.34 $\mu$g/mL (150 times dilution). A high density alignment (~18 SWNT/$\mu$m) is shown in the Figure 4e,f. To achieve this alignment, the original solution was diluted 10-fold (5 $\mu$g/mL). The quality and density of the alignment of the SWNT do not exhibit any noticeable differences as $L$ was increased from 2 to 10 $\mu$m. From these images, it can be seen that the electrode gap is mostly bridged by individual nanotubes irrespective of the different electrode gaps. The DEP process most likely favors the alignment of the nanotube of length comparable to $L$, although in larger channel length devices, a few of them are bridged by multiply connected nanotubes.

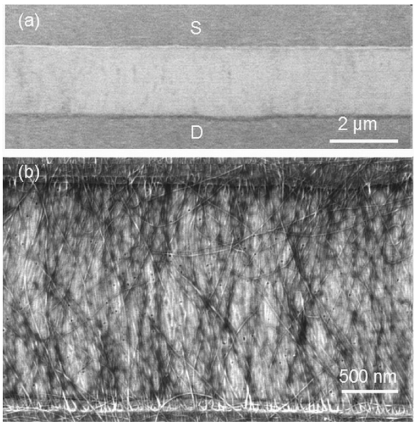


**Figure 3. (a) SEM image of a densely packed array. (b) Magnified image to show that some nanotubes form a second or third layer.**

Our DEP assembly technique can also be extended to a homogeneously aligned SWNT for large channel width devices. Figure 5 shows the aligned array of nanotubes with SWNT density of 20 SWNT/$\mu$m on various channel width devices of $W$ = 100, 500, and 1000 $\mu$m. We found that the linear density of the SWNT is independent of $W$ when all DEP parameters were kept fixed, except that the volume of the solution droplet needs to be increased. We noticed that the assembly is fairly uniform over the entire channel width.

Figure 6 summarizes the density of nanotubes in aligned arrays *versus* concentration of the SWNT solution for different channel lengths of $L$ = 2, 5, and 10 $\mu$m. The

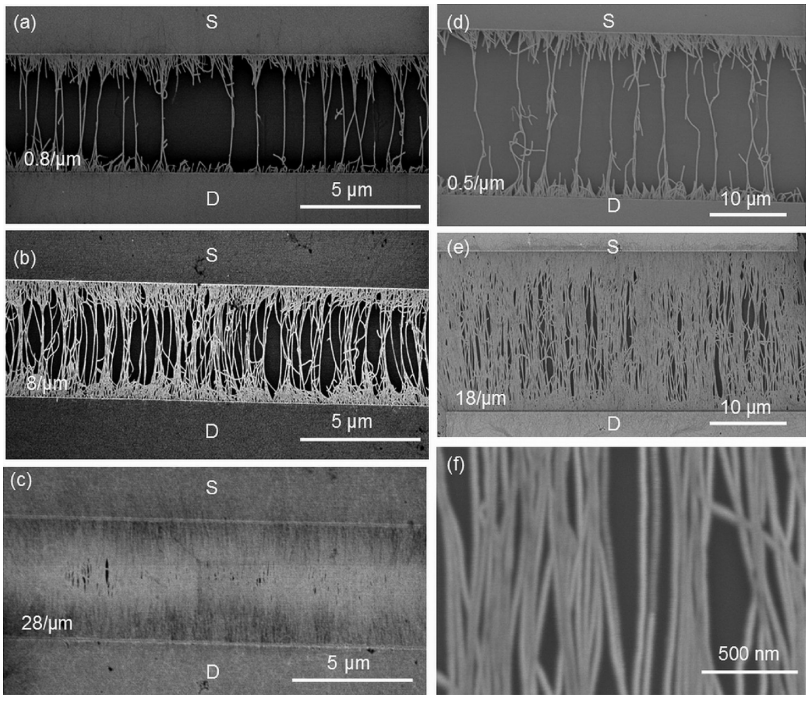


**Figure 4. DEP assembly using higher channel length of 5 and 10 $\mu$m with tunable nanotube density. (a−c) SEM image showing ~1, 8, and 28 SWNT/$\mu$m in 5 $\mu$m channel length device. (d,e) SEM image showing ~0.5 and 18 SWNT/$\mu$m. (f) Magnified image of (e).**

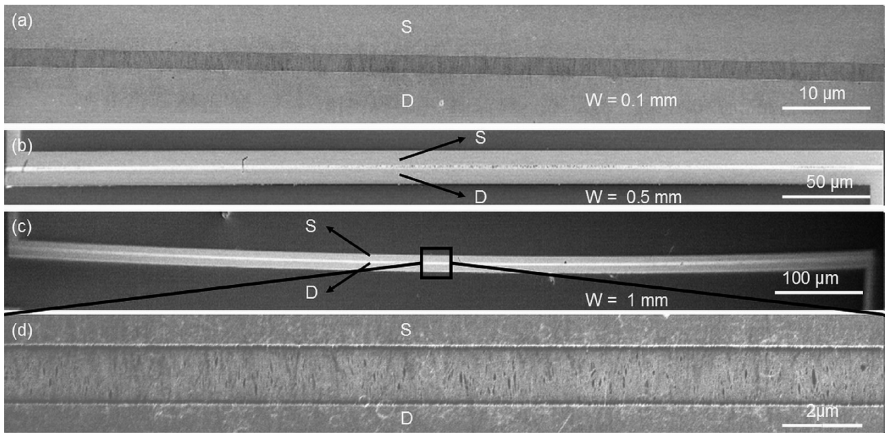


**Figure 5. SEM image showing homogeneous assembly of SWNTs on large channel width devices of $L = 2\ \mu$m, (a) $W = 0.1$ mm (100 $\mu$m); (b) $W = 0.5$ mm (500 $\mu$m); (c) $W = 1$ mm. (d) Enlarged view of (c). Average density of SWNTs is 20/$\mu$m in all of the images.**

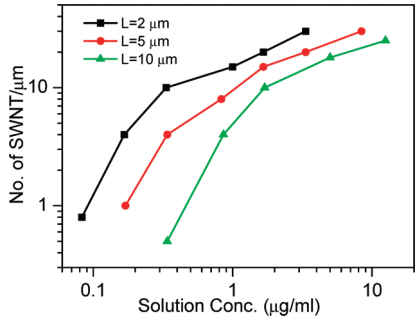


**Figure 6. Variation of the linear density of SWNTs in the array during DEP assembly with concentration of SWNT solution for different channel length devices.**

DEP parameters were fixed, but the effective electric field reduces with increasing $L$. For this reason, to achieve comparable alignment in $L = 5$ and 10 $\mu$m with that of the $L = 2\ \mu$m device, a higher concentration of SWNT is required. For example, to achieve the density of 4 SWNT/$\mu$m on $L = 2$, 5, and 10 $\mu$m, the concentration of SWNT solution requirement varies as 0.167, 0.34, and 0.86 $\mu$g/mL, respectively. There seems to be a tendency that with increasing concentration the linear density of SWNTs in the array initially increases rapidly and becomes much slower at higher densities (saturation in log−log scale). After about 30 SWNT/$\mu$m, we observe formation of double layers. It is interesting to note that, even in the double growth CVD method, the maximum density did not exceed 30 SWNT/$\mu$m.[18]

We have examined the electrical characteristics of the assembled devices. Before electrical characterization, the devices were annealed at 200 °C in Ar/$H_2$ atmosphere for an hour to reduce the contact resistance. Figure 7a shows the typical current−voltage ($I$−$V$) characteristics for a high density (20 SWNT/$\mu$m) alignment. At low bias, the $I$−$V$ curves are linear for all channel lengths, indicating Ohmic contact with Pd electrodes. The resistance ($R$) values were found to be 500 Ω, 1 kΩ, and 1.5 kΩ, respectively, for $L = 2$, 5, and 10 $\mu$m, respectively. Figure 7b shows a plot of device resistance (after

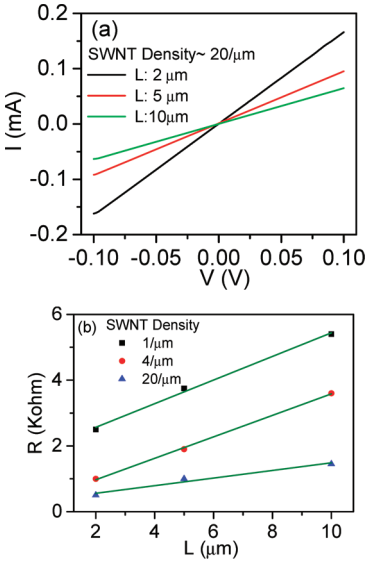


**Figure 7. (a) $I$−$V$ curves for the SWNT array with ~20 SWNT/$\mu$m. (b) Resistance of the array *versus* channel length $L$ for different SWNT density.**

annealing) *versus* channel length for low, medium, and high packing density of SWNTs. For the same packing density, the $R$ increases almost linearly with increasing channel length. $R$ per unit length remains constant for all cases. Since the device resistance is the sum of contact resistance ($R_{contact}$) and channel resistance ($R_{channel}$), we can estimate both parameters from these curves. The contact and sheet resistance is related by the equation $R = R_{contact} + R_{channel}$[11], where $R_{channel} = R_{sheet}(L/W)$. We obtain values of $R_{contact} \sim 2315$, 380, and 330 Ω for low (1/$\mu$m), medium (4/$\mu$m), and high densities (20/$\mu$m), respectively. The sheet resistance is calculated from the slope of linear fits, and their values were 8.8, 8.1, and 2.9 kΩ/□ for low, medium, and high densities, respectively. These sheet resistance values are much lower compared to the thin film of random nanotubes or nanotube cross bar junctions.[42] The low sheet resistance demonstrates that our aligned array has potential application as an

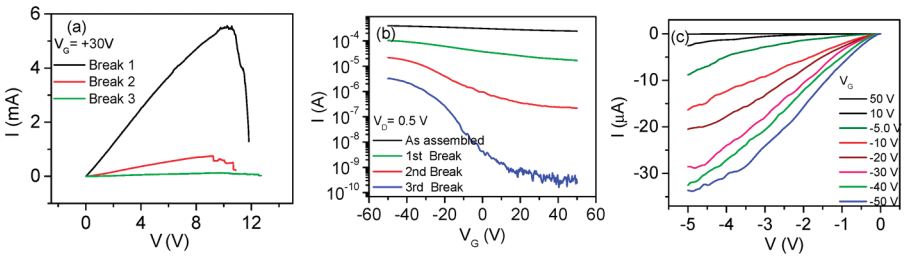


**Figure 8. (a) *I*−*V* characteristics for three sequential electrical breakdowns. *I* was allowed to fall by an order of magnitude during the first two breakdowns, after which the voltage was swept back to zero. (b) *I vs* $V_G$ (back gate voltage) at constant *V* of 0.5 V after each breakdown. The on−off ratio improves after each breakdown due to removal of metallic pathways. (c) Output characteristics of the FET after the third breakdown.**

electrode material for different applications, such as organic electronics and photovoltaics.[12,29]

In previous DEP studies of SWNTs, it was claimed that DEP assembly favors metallic (m) SWNTs over semiconducting (s) SWNTs. The low sheet resistance therefore raises the question whether the assembly contains any s-SWNT. In order to investigate this, we have used selective removal of metallic nanotubes using an electrical breakdown technique and checked if field-effect transistors (FETs) can be fabricated using the remaining s-SWNTs. Figure 8a shows the representative *I*−*V* plot for three sequential breakdowns for one of our devices with 20 SWNT/$\mu$m and $L = 5\ \mu$m. The back gate was held constant at $V_G = +30$ V to deplete the carriers in the p-type semiconducting SWNTs, while we ramped up *V* to eliminate the metallic SWNTs. As *V* was ramped up, the SWNTs started to break down and *I* began to fall. In order to obtain reproducible results, each breakdown was stopped when *I* had fallen by an order of magnitude and at that point *V* was swept back to zero. Figure 8b shows the variation of *I* as a function of $V_G$ after each breakdown. The bias (*V*) was kept constant at 0.5 V. The mobility ($\mu$) was calculated by using the formula $\mu = (L/WVC) \times (dI/dV_G)$. The capacitance per unit area *C* is calculated by using the formula for a parallel nanotube array, $C = D/[C_Q^{-1} + (1/2\pi\varepsilon_0\varepsilon)\ln[\sinh(2\pi t_{ox}D)/\pi Dr]]$, where $\varepsilon$ is the dielectric constant of $SiO_2$, $t_{ox} = 250$ nm is the thickness of $SiO_2$, $C_Q = 4 \times 10^{-10}$ F/m is the quantum capacitance, *r* is the radius of the nanotubes, and *D* is the linear density in SWNTs per $\mu$m of the array.[10] The as-assembled array shows very little gate modulation with current on−off ratio of 1.5 and corresponding mobility of ~50 $cm^2/(V\cdot s)$ due to the presence of large numbers of metallic pathways. After the first breakdown, the FET behavior of the device is enhanced with an on−off ratio ~10 and $\mu \sim 30$ $cm^2/(V\cdot s)$. After the second breakdown, the on−off ratio increased to ~100 with $\mu \sim 20$ $cm^2/(V\cdot s)$. Finally, after the third breakdown, the on−off ratio increases to $\sim 1.3 \times 10^4$ with $\mu \sim 10$ $cm^2/(V\cdot s)$. The mobility drops slightly from breakdown to breakdown due to the reduced current from the removal of metallic nanotubes, which in turn reduces the transconductance. Figure 8c shows the output characteristics, *I versus V* at different $V_G$ recorded for the same sample after the third breakdown. Supporting Information Figure S3 summarizes the device property for two nanotube densities of 4 and 20 SWNT/$\mu$m. A more systematic study of FET properties with different density in the array is under investigation. However, our results clearly show that both m-SWNTs and s-SWNTs are present in our aligned array devices and that m-SWNTs can be selectively removed to fabricate FET.

In conclusion, we have demonstrated ultrahigh density alignment of SWNTs in an array using high-quality SWNT aqueous solution and dielectrophoresis. By tuning the concentration of the SWNT solution, we can control the density of the nanotube up to 30 SWNT/$\mu$m in the array, which is the highest reported density using any solution processing technique. Effort to further increase the density resulted in multiple layers of nanotubes in the array. Electrical measurement data show that the densely packed aligned arrays have low sheet resistances. Selective removal of metallic SWNTs *via* controlled electrical breakdown produced field-effect transistors with high current on−off ratio. Ultrahigh density alignment using solution processed SWNTs reported here will have important implication in fabricating high-quality nanoelectronic devices.

## MATERIALS AND METHODS

Devices were fabricated on heavily doped silicon substrates capped with a thermally grown 250 nm thick $SiO_2$ layer. The electrode patterns were fabricated by a combination of optical and electron beam lithography (EBL). First, contact pads and electron beam markers were fabricated with optical lithography using double layer resists (LOR 3A/Shipley 1813) developing in CD26, thermal evaporation of 3 nm chromium (Cr) and 50 nm gold (Au) followed by lift-off. Smaller electrode patterns were fabricated with EBL using single-layer PMMA resists and then developing in (1:3) methyl isobutyl ketone/isopropyl alchohol (MIBK/IPA). After

defining the patterns, 3 nm Cr and 27 nm thick Pd were deposited using electron beam deposition followed by lift-off in boiling acetone. Pd was used because it is known to make the best electrical contact to SWNTs. The channel lengths ($L$) were 2, 5, and 10 $\mu$m, while the channel width ($W$) was varied from 25 $\mu$m to 1 mm. There are nine independent drain and source (electrodes) pairs on each chip.

The devices were imaged using a Zeiss Ultra 55 field emission scanning electron microscope. The microscope is capable of delivering high lateral resolution at low voltages. Inlens detector was used to get the image at low voltages. The electrical measurements were performed in a probe station by a high-resolution DAC card and a current preamplifier (DL1211) interfaced with LabView.

*Acknowledgment.* This work is partially supported by the U.S. National Science Foundation under Grant ECCS-0748091 (CAREER).

*Supporting Information Available:* SEM and AFM images of the nanotubes dispersed on $Si/SiO_2$ and mica substrates along with length and diameter distributions, simulation of nanotube assembly and affect of short nanotubes, FET characteristics with electrical breakdown, and SEM image after electrical breakdown. This material is available free of charge *via* the Internet at http://pubs.acs.org.

## REFERENCES AND NOTES


1. Saito, R.; Dresselhaus, G.; Dresselhaus, M. S. *Physical Properties of Carbon Nanotubes*; World Scientific: Singapore, 1998.
2. Avouris, P.; Chen, Z.; Perebeinos, V. Carbon-Based Electronics. *Nat. Nanotechnol.* **2007,** *2*, 605–615.
3. Durkop, T.; Getty, S. A.; Cobas, E.; Fuhrer, M. S. Extraordinary Mobility in Semiconducting Carbon Nanotubes. *Nano Lett.* **2004,** *4*, 35–39.
4. Javey, A.; Guo, J.; Wang, Q.; Lundstrom, M.; Dai, H. Ballistic Carbon Nanotube Field-Effect Transistor. *Nature* **2003,** *424*, 654–657.
5. Rutherglen, C.; Jain, D.; Burke, P. Nanotube Electronics for Radio Frequency Applications. *Nat. Nanotechnol.* **2009,** *4*, 811–819.
6. Kocabas, C.; Hur, S.-H.; Gaur, A.; Meitl, M. A.; Shim, M.; Rogers, J. A. Guided Growth of Large-Scale, Horizontally Aligned Arrays of Single-Walled Carbon Nanotubes and Their Use in Thin-Film Transistors. *Small* **2005,** *1*, 1110–1116.
7. Kocabas, C.; Kim, H.-s.; Banks, T.; Rogers, J. A.; Pesetski, A. A.; Baumgardner, J. E.; Krishnaswamy, S. V.; Zhang, H. Radio Frequency Analog Electronics Based on Carbon Nanotube Transistors. *Proc. Natl. Acad. Sci. U.S.A.* **2008,** *105*, 1405–1409.
8. Rutherglen, C.; Jain, D.; Burke, P. RF Resistance and Inductance of Massively Parallel Single Walled Carbon Nanotubes: Direct, Broadband Measurements and Near Perfect 50 Ω Impedance Matching. *Appl. Phys. Lett.* **2008,** *93*, 083119-1–083119-3.
9. Pesetski, A. A.; Baumgardner, J. E.; Krishnaswamy, S. V.; Zhang, H.; Adam, J. D.; Kocabas, C.; Banks, T.; Rogers, J. A. A 500 MHz Carbon Nanotube Transistor Oscillator. *Appl. Phys. Lett.* **2008,** *93*, 123506-1–123506-3.
10. Kang, S. J.; Kocabas, C.; Ozel, T.; Shim, M.; Pimparkar, N.; Alam, M. A.; Rotkin, S. V.; Rogers, J. A. High-Performance Electronics Using Dense, Perfectly Aligned Arrays of Single-Walled Carbon Nanotubes. *Nat. Nanotechnol.* **2007,** *2*, 230–236.
11. Ishikawa, F. N.; Chang, H.-k.; Ryu, K.; Chen, P.-c.; Badmaev, A.; De Arco, L. G.; Shen, G.; Zhou, C. Transparent Electronics Based on Transfer Printed Aligned Carbon Nanotubes on Rigid and Flexible Substrates. *ACS Nano* **2008,** *3*, 73–79.
12. Cao, Q.; Rogers, J. A. Ultrathin Films of Single-Walled Carbon Nanotubes for Electronics and Sensors: A Review of Fundamental and Applied Aspects. *Adv. Mater.* **2009,** *21*, 29–53.
13. Kim, S.; Ju, S.; Back, J. H.; Xuan, Y.; Ye, P. D.; Shim, M.; Janes, D. B.; Mohammadi, S. Fully Transparent Thin-Film Transistors Based on Aligned Carbon Nanotube Arrays and Indium Tin Oxide Electrodes. *Adv. Mater.* **2009,** *21*, 564–568.
14. Zhou, W.; Rutherglen, C.; Burke, P. J. Wafer Scale Synthesis of Dense Aligned Arrays of Single-Walled Carbon Nanotubes. *Nano Res.* **2008,** *1*, 158–165.
15. Kocabas, C.; Dunham, S.; Cao, Q.; Cimino, K.; Ho, X.; Kim, H.-S.; Dawson, D.; Payne, J.; Stuenkel, M.; Zhang, H.; Banks, T.; Feng, M.; Rotkin, S. V.; Rogers, J. A. High-Frequency Performance of Submicrometer Transistors That Use Aligned Arrays of Single-Walled Carbon Nanotubes. *Nano Lett.* **2009,** *9*, 1937–1943.
16. Ryu, K.; Badmaev, A.; Wang, C.; Lin, A.; Patil, N.; Gomez, L.; Kumar, A.; Mitra, S.; Wong, H.-S. P.; Zhou, C. CMOS-Analogous Wafer-Scale Nanotube-on-Insulator Approach for Submicrometer Devices and Integrated Circuits Using Aligned Nanotubes. *Nano Lett.* **2009,** *9*, 189–197.
17. McNicholas, T. P.; Ding, L.; Yuan, D.; Liu, J. Density Enhancement of Aligned Single-Walled Carbon Nanotube Thin Films on Quartz Substrates by Sulfur-Assisted Synthesis. *Nano Lett.* **2009,** *9*, 3646–3650.
18. Hong, S. W.; Banks, T.; Rogers, J. A. Improved Density in Aligned Arrays of Single-Walled Carbon Nanotubes by Sequential Chemical Vapor Deposition on Quartz. *Adv. Mater.* **2010,** *22*, 1826–1830.
19. Li, X.; Zhang, L.; Wang, X.; Shimoyama, I.; Sun, X.; Seo, W.-S.; Dai, H. Langmuir−Blodgett Assembly of Densely Aligned Single-Walled Carbon Nanotubes from Bulk Materials. *J. Am. Chem. Soc.* **2007,** *129*, 4890–4891.
20. Yu, G.; Cao, A.; Lieber, C. M. Large-Area Blown Bubble Films of Aligned Nanowires and Carbon Nanotubes. *Nat. Nanotechnol.* **2007,** *2*, 372–377.
21. Tang, G.; Zhang, X.; Yang, S.; Derycke, V.; Benattar, J.-J. New Confinement Method for the Formation of Highly Aligned and Densely Packed Single-Walled Carbon Nanotube Monolayers. *Small* **2010,** *6*, 1488–1491.
22. Engel, M.; Small, J. P.; Steiner, M.; Freitag, M.; Green, A. A.; Hersam, M. C.; Avouris, P. Thin Film Nanotube Transistors Based on Self-Assembled, Aligned, Semiconducting Carbon Nanotube Arrays. *ACS Nano* **2008,** *2*, 2445–2452.
23. LeMieux, M. C.; Roberts, M.; Barman, S.; Jin, Y. W.; Kim, J. M.; Bao, Z. Self-Sorted, Aligned Nanotube Networks for Thin-Film Transistors. *Science* **2008,** *321*, 101–104.
24. Liu, H.; Takagi, D.; Chiashi, S.; Homma, Y. Transfer and Alignment of Random Single-Walled Carbon Nanotube Films by Contact Printing. *ACS Nano* **2010,** *4* 933–938.
25. Stokes, P.; Silbar, E.; Zayas, Y. M.; Khondaker, S. I. Solution Processed Large Area Field Effect Transistors from Dielectrophoreticly Aligned Arrays of Carbon Nanotubes. *Appl. Phys. Lett.* **2009,** *94*, 113104-1–113104-3.
26. Nougaret, L.; Happy, H.; Dambrine, G.; Derycke, V.; Bourgoin, J.-P.; Green, A. A.; Hersam, M. C. 80 GHz Field-Effect Transistors Produced Using High Purity Semiconducting Single-Walled Carbon Nanotubes. *Appl. Phys. Lett.* **2009,** *94*, 243505-1–243505-3.
27. Opatkiewicz, J.; LeMieux, M. C.; Bao, Z. Nanotubes on Display: How Carbon Nanotubes Can Be Integrated into Electronic Displays. *ACS Nano* **2010,** *4*, 2975–2978.
28. Wang, C.; Zhang, J.; Ryu, K.; Badmaev, A.; De Arco, L. G.; Zhou, C. Wafer-Scale Fabrication of Separated Carbon Nanotube Thin-Film Transistors for Display Applications. *Nano Lett.* **2009,** *9*, 4285–4291.
29. Feng, C.; Liu, K.; Wu, J.-S.; Liu, L.; Cheng, J.-S.; Zhang, Y.; Sun, Y.; Li, Q.; Fan, S.; Jiang, K. Flexible, Stretchable, Transparent Conducting Films Made from Superaligned Carbon Nanotubes. *Adv. Funct. Mater.* **2010,** *20*, 885–891.
30. Kim, S. N.; Rusling, J. F.; Papadimitrakopoulos, F. Carbon Nanotubes for Electronic and Electrochemical Detection of Biomolecules. *Adv. Mater.* **2007,** *19*, 3214–3228.
31. Monica, A. H.; Papadakis, S. J.; Osiander, R.; Paranjape, M. Wafer-Level Assembly of Carbon Nanotube Networks Using Dielectrophoresis. *Nanotechnology* **2008,** *19*, 085303-1–085303-5.

32. Krupke, R.; Linden, S.; Rapp, M.; Hennrich, F. Thin Films of Metallic Carbon Nanotubes Prepared by Dielectrophoresis. *Adv. Mater.* **2006,** *18*, 1468–1470.
33. Khondaker, S. I. Fabrication of Nanoscale Device Using Individual Colloidal Gold Nanoparticle. *IEE Proc. Circuits, Devices Syst.* **2004,** *151*, 457–460.
34. Joung, D.; Chunder, A.; Zhai, L.; Khondaker, S. I. High Yield Fabrication of Chemically Reduced Graphene Oxide Field Effect Transistor by Dielectrophoresis. *Nanotechnology* **2010,** *21*, 165202-1–165202-5.
35. Stokes, P.; Khondaker, S. I. Local-Gated Single-Walled Carbon Nanotube Field Effect Transistors Assembled by AC Dielectrophoresis. *Nanotechnology* **2008,** *17*, 175202-1–175202-5.
36. Stokes, P.; Khondaker, S. I. High Quality Solution Processed Carbon Nanotube Transistors Assembled by Dielectrophoresis. *Appl. Phys. Lett.* **2010,** *96*, 083110-1–083110-3.
37. Stokes, P.; Khondaker, S. I. Evaluating Defects in Solution Processed Carbon Nanotube Devices *via* Low Temperature Transport Spectroscopy. *ACS Nano* **2010,** *4*, 2659–2666.
38. Vijayaraghavan, A.; Blatt, S.; Weissenberger, D.; Oron-Carl, M.; Hennrich, F.; Gerthsen, D.; Hahn, H.; Krupke, R. Ultra-Large-Scale Directed Assembly of Single-Walled Carbon Nanotube Devices. *Nano Lett.* **2007,** *7*, 1556–1560.
39. Brewer Science Inc. http://www.brewerscience.com/products/carbon-nanotube/ (Accessed September 6, 2010).
40. Sen, R.; Sivarajan R.; Rueckes T.; Segal, B. M. High Purity Nanotube Fabrics and Films; U.S. Patent 0058797 A1; Nantero, Inc., Woburn, MA, March 17, 2005.
41. Dimaki, M.; Boggild, P. Dielectrophoresis of Carbon Nanotubes Using Microelectrodes: A Numerical Study. *Nanotechnology* **2004,** *15*, 1095–1102.
42. Kang, S. J.; Kocabas, C.; Kim, H.-S.; Cao, Q.; Meitl, M. A.; Khang, D.-Y.; Rogers, J. A. Printed Multilayer Superstructures of Aligned Single-Walled Carbon Nanotubes for Electronic Applications. *Nano Lett.* **2007,** *7*, 3343–3348.